ROYAL SOCIETY OF CHEMISTRY

COMMUNICATION

Check for updates

Transient changes in aromaticity and their effect on excited-state proton transfer reactions†

Enrique M. Arpa (ID) * and Bo Durbeej (ID) *

The common approach to investigate the impact of aromaticity on excited-state proton transfer by probing the (anti)aromatic character of reactants and products alone is scrutinized by modelling such reactions involving 2-pyridone. Thereby, it is found that energy barriers can be strongly influenced by transient changes in aromaticity unaccounted for by this approach, particularly when the photoexcited state interacts with a second excited state. Overall, the modelling identifies a pronounced effect overlooked by most studies on this topic.

Excited-state aromaticity (ESA) and antiaromaticity (ESAA) are powerful concepts for rationalizing the behavior of cyclic, conjugated π-electron systems in electronically excited states.[1–4] Similarly to their ground-state counterparts, these concepts help clarify trends in stability and/or reactivity in terms of gains or losses of (anti)aromatic character. While it may be a challenging task to quantify ESA and ESAA using experimental tools alone, aromaticity indices obtained computationally to probe these features in ground states are also useful for studies of excited states. Accordingly, standard indices, such as the nucleus-independent chemical shift (NICS),[5,6] the Shannon aromaticity[7] and the harmonic oscillator model for aromaticity (HOMA)[8] indices, can provide information about ESA and ESAA from calculated excited-state wave functions, electron densities and geometries, respectively. For example, based on such calculations, many insights have been derived regarding both the design of molecular photoswitches,[9–12] light-driven molecular motors[13,14] and singlet-fission materials,[15,16] and the driving forces for photochemical planarization reactions.[17,18]

One type of photochemical reactions of widespread interest from the viewpoint of aromaticity considerations is excited-state proton transfer (ESPT),[19–22] which plays a key role for many photobiological processes[23,24] and is commonly exploited for the rational design of molecules with unique photoresponsive

Division of Theoretical Chemistry, IFM, Linköping University, SE-581 83, Linköping, Sweden. E-mail: enrique.arpa@liu.se, bodur@ifm.liu.se

† Electronic supplementary information (ESI) available: Computational details, complementary results (Fig. S1–S25 and Table S1) and Cartesian coordinates and energies of molecular geometries. See DOI: https://doi.org/10.1039/d2cp00494a

properties.[25–27] Specifically, when the proton donor/acceptor is a π-conjugated ring, ESA and ESAA help unravel the equilibrium between the species transformed by the proton transfer. Similarly, gains in ESA or losses in ESAA have been identified as the driving force for such reactions in many different systems, both when occurring independently[28–31] or coupled to other processes.[32,33] Yet, with few exceptions,[32] analyses undertaken to investigate the effect of aromaticity on these reactions have usually focused on the (anti)aromatic character of the reactants and products alone. However, while such a procedure is sensible for assessing how aromaticity influences the overall thermodynamics of the processes, it does not account for the role attributable to aromaticity changes along the reaction coordinate, or for the effect of aromaticity on the reaction kinetics. Indeed, a more complete picture of how ESA and ESAA determine the fate of ESPT reactions requires that numerous molecular structures along the reaction coordinate are considered.

In this work, we present a comparison of the aforementioned standard procedure to probe the impact of ESA and ESAA on ESPT reactions based exclusively on (anti)aromatic signatures of reactants and products, with a more thorough approach that additionally examines the gradual changes in such signatures during the conversion of reactants into products. To this end, we perform quantum chemical calculations with a combination of time-dependent density functional theory (TD-M06-2X[34]) and multiconfigurational *ab initio* (CASSCF[35] and XMS-CASPT2[36]) methods to model a set of different ESPT reactions involving 2-pyridone, each of which is depicted in Fig. 1 and occurs in the lowest singlet excited state (S_1). Thereby, it is demonstrated that while the standard procedure is perfectly sensible in some instances, it becomes of limited use when the localization or the charge-transfer (CT) character of the S_1 state changes during the course of the reaction. Given that it is difficult to rule out these scenarios based on calculations that merely consider the reactant and product species, it is concluded that the influence of ESA and ESAA on ESPT reactions is best investigated by mapping of the full reaction coordinate.
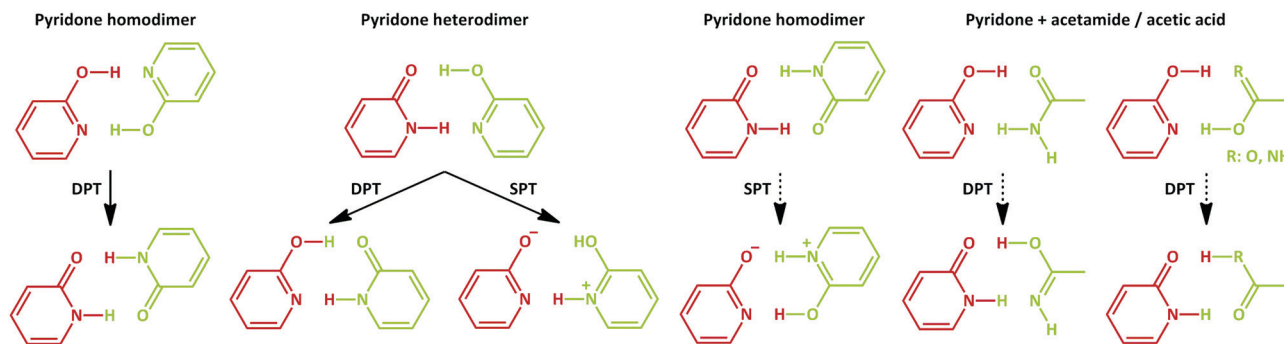
Fig. 1   ESPT reactions studied in this work (the results for the reactions with a dashed arrow are presented in the ESI†). SPT = single proton transfer, DPT = double proton transfer.

As outlined by the computational details given in the ESI,† our investigation makes use of both NICS and HOMA indices to assess the (anti)aromatic character of the ring(s) involved in the ESPT reactions. Below, we will focus on analyses based on the former magnetic index using the NICS-scan procedure described by Stanger, which alleviates the arbitrariness introduced by otherwise having to choose one specific point in space for these calculations.[37] In support of the NICS-scan results, complementary analyses based on the geometric HOMA index are presented in the ESI.† Given that this index is associated with a few pitfalls (see discussion in the ESI†),[38,39] we also found it appropriate to include in the ESI† a further corroboration of the NICS-scan results based on the so-called multicenter index,[40] which has proven accurate in various benchmark tests.[41,42]

First, we investigated the double ESPT in the pyridone homodimer, the dimer in which both pyridone rings reside in the same tautomeric form. In the ground S_0 state, the most stable isomer is the dienol form (the hydroxypyridine dimer), in which both rings are aromatic. However, as can be inferred from Fig. 2 and Fig. S1 in the ESI,† excitation to the S_1 state produces the diketo form in a barrierless fashion via a double proton transfer. The excitation does not spread throughout the dimer, but is located on one of the rings (ring A in Fig. 2, see further Table S1 in the ESI†). Accordingly, upon excitation, only this ring becomes antiaromatic (showing distinctly positive NICS values at large r_{N-H} distances in Fig. 2), whereas the other ring (ring B) retains the aromaticity it exhibits in the S_0 state (showing negative NICS values at large r_{N-H} distances). The double proton transfer then leads to losses of the pronounced antiaromaticity of ring A and the weaker aromaticity of ring B, yielding two non-aromatic pyridone moieties with NICS values close to zero (at the smaller r_{N-H} distances in Fig. 2). Thus, it appears that the driving force for the process is the relief of the antiaromaticity of ring A, which corroborates previous studies aimed at identifying general mechanistic principles for ESPT reactions.[28–31] Furthermore, owing to the observation in Fig. 2 that the antiaromaticity is relieved in a markedly smooth fashion along the reaction coordinate, it is clear that one would have arrived at an identical conclusion through calculations
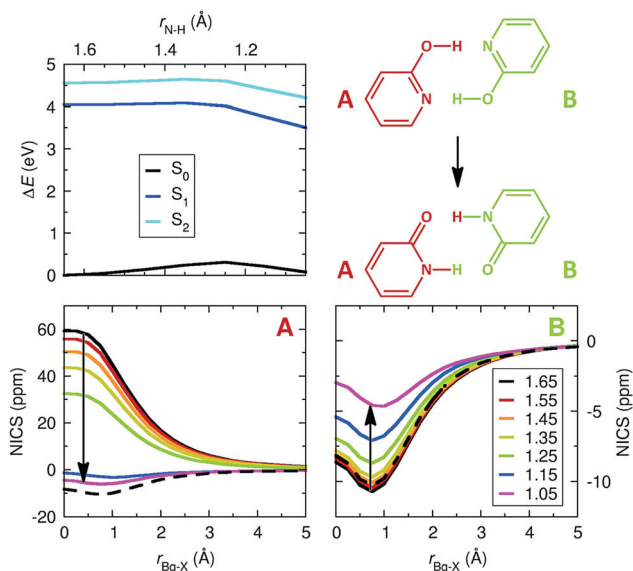

Fig. 2   XMS-CASPT2//TD-M06-2X potential energy (ΔE) curves for the double ESPT in the pyridone homodimer and associated CASSCF NICS values for rings A and B. For the NICS values, full colored curves correspond to values in the S_1 state at different r_{N-H} distances (legends apply to both panels), whereas dashed, black curves correspond to values in the S_0 state of the initial dienol species. Vertical arrows indicate changes in NICS values in the S_1 state during the reaction, and r_{Bq-X} is the distance between the center of the ring in question and the position of the ghost atom utilized for the NICS-scan calculations. These arrows and this distance designation are also used in Fig. 3 and 4.

focusing strictly on the initial dienol and the final diketo species. The same exact implication can be made from the modelling of the double ESPT between hydroxypyridine and acetamide or acetic acid, which is summarized in Fig. S13–S15 in the ESI.†

Turning to the results for the double ESPT in the pyridone heterodimer, which are summarized in Fig. 3 and Fig. S2 in the ESI,† the situation is entirely different. First, in this case, the S_1 state of the initial keto-A-enol-B species is characterized by both rings having the same aromatic signatures as in the S_0 state, with ring A being non-aromatic and ring B being weakly aromatic, as can be inferred from the corresponding NICS
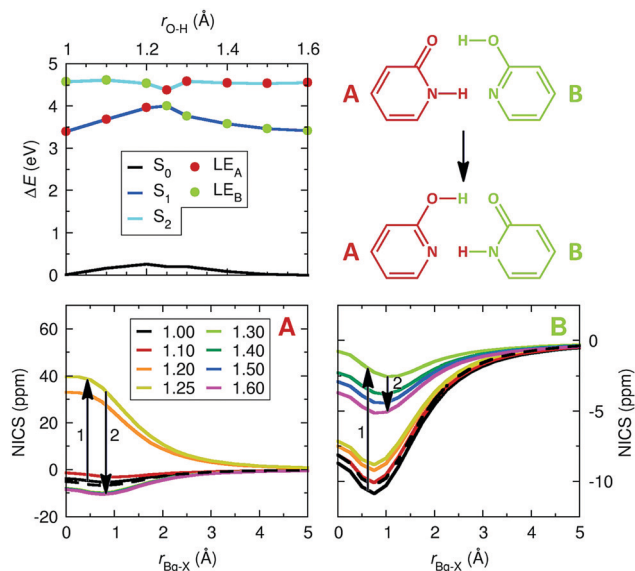
Fig. 3 XMS-CASPT2//TD-M06-2X potential energy (ΔE) curves for the double ESPT in the pyridone heterodimer and associated CASSCF NICS values for rings A and B. For the NICS values, full colored curves correspond to values in the S_1 state at different r_{O-H} distances, whereas dashed, black curves correspond to values in the S_0 state of the initial keto-A-enol-B species. LE = local excitation. Further details are given in the caption for Fig. 2.

values being close to zero and slightly negative, respectively, at small r_{O-H} distances in Fig. 3. This is because the moiety on which the excitation is located (ring A, see further Table S1, ESI†) is non-aromatic. Second, the double proton transfer

Fig. 4 XMS-CASPT2//TD-M06-2X potential energy (ΔE) curves for the single ESPT in the pyridone heterodimer and associated CASSCF NICS values for rings A and B. For the NICS values, full colored curves correspond to values in the S_1 state at different r_{N-H} distances, whereas dashed, black curves correspond to values in the S_0 state of the initial keto-A-enol-B species. LE = local excitation, $CT_{A \to B}$ = A → B CT state. Further details are given in the caption for Fig. 2.

changes the localization of the excitation from ring A to ring B, whereby ring A becomes weakly aromatic and ring B non-aromatic in the S_1 state of the resulting enol-A-keto-B isomer. Owing to this process, which appears to be mediated by the exchange of "diabatic" character between the S_1 and S_2 states in a diabatic crossing (see Fig. 3), the changes in aromaticity along the reaction coordinate are not smooth – rather, they are sudden and sharp, as highlighted by the vertical arrows in Fig. 3. Specifically, as the crossing is approached, ring A develops pronounced antiaromaticity, but only transiently as it reaches its final state of weak aromaticity after the crossing is bypassed. This explains why the overall ESPT reaction is predicted to have an appreciable barrier of 0.61 eV. Clearly, had the calculations been based on the reactants and products alone, this key finding on the role of transient antiaromaticity would not have been made.

A second example that a thorough assessment of how aromaticity controls ESPT reactions requires mapping of the full reaction coordinate is given in Fig. 4, which shows the single ESPT between the nitrogen centers of the pyridone heterodimer. This system can be thought of as a simplified model of Watson–Crick base pairing, for which aromaticity-driven proton-coupled electron transfer has been proposed as one possible non-radiative decay funnel to the S_0 state.[24] During the single proton transfer, the nature of the S_1 state changes from a local excitation on ring A (LE_A) at the initial species to an A → B CT state ($CT_{A \to B}$) as the reaction progresses (see further Table S1, ESI†). Similarly to the situation for the double ESPT, this change is mediated by the exchange of "diabatic" character between the S_1 and S_2 states, which again results in sudden, sharp increases and decreases in the (anti)-aromatic character of the two rings along the reaction coordinate (see the vertical arrows in Fig. 4). Indeed, as the crossing is approached, ring A develops transient antiaromaticity and ring B loses aromaticity, which introduces a barrier of 0.62 eV for the overall ESPT reaction. Once the crossing is bypassed, however, ring A returns to being non-aromatic, whereas ring B turns antiaromatic. Thus, once again, it is clear that the impact of aromaticity on ESPT reactions cannot be fully appreciated without considering the full reaction coordinate.

Conclusions

In summary, we have shown that the commonly employed strategy to investigate the influence of aromaticity on ESPT reactions based exclusively on (anti)aromatic signatures of reactants and products warrants caution. For reactions where neither the localization nor the CT character of the photoexcited state changes as the reactions proceed, this strategy is found to provide sufficient insight into the effect of aromaticity. However, for reactions where these conditions are not fulfilled, the strategy fails to unveil transient changes in aromaticity that might significantly influence energy barriers. Since there is no way of knowing beforehand without performing actual calculations whether a specific ESPT reaction meets the necessary
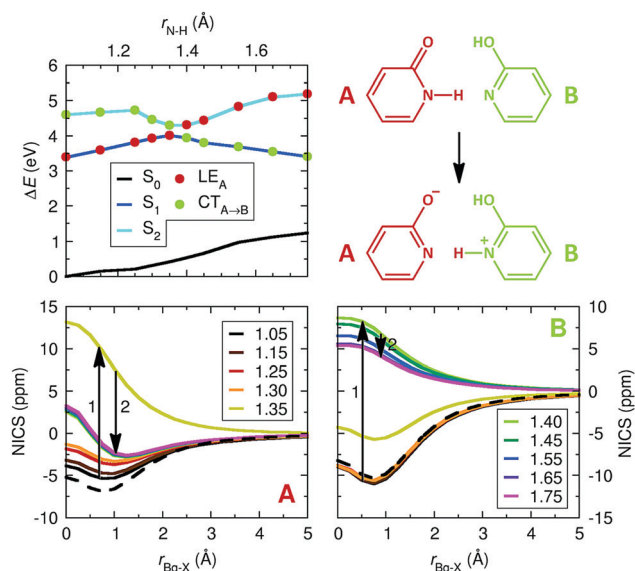
11498 | *Phys. Chem. Chem. Phys.*, 2022, **24**, 11496–11500

This journal is © the Owner Societies 2022

requirements in this regard, we propose that more detailed calculations that also account for intermediate structures along the reaction coordinate become the new norm for exploring how ESA and ESAA control ESPT reactions. Moreover, although our study focuses on ESPT reactions, it seems reasonable to expect that the present results are relevant also for studies of the general photoreactivity of π-conjugated rings.

Author contributions

The authors contributed equally to all parts of this work.

Conflicts of interest

There are no conflicts to declare.

Acknowledgements

References

1 N. C. Baird, *J. Am. Chem. Soc.*, 1972, **94**, 4941–4948.

2 H. Ottosson, *Nat. Chem.*, 2012, **4**, 969–971.

3 M. Rosenberg, C. Dahlstrand, K. Kilså and H. Ottosson, *Chem. Rev.*, 2014, **114**, 5379–5425.

4 M. Hada, S. Saito, S. Tanaka, R. Sato, M. Yoshimura, K. Mouri, K. Matsuo, S. Yamaguchi, M. Hara, Y. Hayashi, F. Röhricht, R. Herges, Y. Shigeta, K. Onda and R. J. D. Miller, *J. Am. Chem. Soc.*, 2017, **139**, 15792–15800.

5 P. v. R. Schleyer, C. Maerker, A. Dransfeld, H. Jiao and N. J. R. van Eikema Hommes, *J. Am. Chem. Soc.*, 1996, **118**, 6317–6318.

6 H. Fallah-Bagher-Shaidaei, C. S. Wannere, C. Corminboeuf, R. Puchta and P. V. R. Schleyer, *Org. Lett.*, 2006, **8**, 863–866.

7 S. Noorizadeh and E. Shakerzadeh, *Phys. Chem. Chem. Phys.*, 2010, **12**, 4742–4749.

8 J. Kruszewski and T. M. Krygowski, *Tetrahedron Lett.*, 1972, **13**, 3839–3842.

9 H. Löfås, B. O. Jahn, J. Wärnå, R. Emanuelsson, R. Ahuja, A. Grigoriev and H. Ottosson, *Faraday Discuss.*, 2014, **174**, 105–124.

10 B. Durbeej, J. Wang and B. Oruganti, *ChemPlusChem*, 2018, **83**, 958–967.

11 A. B. Skov, N. Ree, A. S. Gertsen, P. Chabera, J. Uhlig, J. S. Lissau, L. Nucci, T. Pullerits, K. V. Mikkelsen, M. B. Nielsen, T. I. Sølling and T. Hansen, *ChemPhotoChem*, 2019, **3**, 619–629.

12 B. Oruganti, P. P. Kalapos, V. Bhargav, G. London and B. Durbeej, *J. Am. Chem. Soc.*, 2020, **142**, 13941–13953.

13 B. Oruganti, J. Wang and B. Durbeej, *Org. Lett.*, 2017, **19**, 4818–4821.

14 J. Wang, B. Oruganti and B. Durbeej, *ChemPhotoChem*, 2019, **3**, 450–460.

15 K. J. Fallon, P. Budden, E. Salvadori, A. M. Ganose, C. N. Savory, L. Eyre, S. Dowland, Q. Ai, S. Goodlett, C. Risko, D. O. Scanion, C. W. M. Kay, A. Rao, R. H. Friend, A. J. Musser and H. Bronstein, *J. Am. Chem. Soc.*, 2019, **141**, 13867–13876.

16 O. El Bakouri, J. R. Smith and H. Ottosson, *J. Am. Chem. Soc.*, 2020, **142**, 5602–5617.

17 J. Toldo, O. El Bakouri, M. Solà, P.-O. Norrby and H. Ottosson, *ChemPlusChem*, 2019, **84**, 712–721.

18 R. Kotani, L. Liu, P. Kumar, H. Kuramochi, T. Tahara, P. Liu, A. Osuka, P. B. Karadakov and S. Saito, *J. Am. Chem. Soc.*, 2020, **142**, 14985–14992.

19 L. G. Arnaut and S. J. Formosinho, *J. Photochem. Photobiol., A*, 1993, **75**, 1–20.

20 S. J. Formosinho and L. G. Arnaut, *J. Photochem. Photobiol., A*, 1993, **75**, 21–48.

21 S. Scheiner, *J. Phys. Chem. A*, 2000, **104**, 5898–5909.

22 N. Agmon, *J. Phys. Chem. A*, 2005, **109**, 13–35.

23 M. Chattoraj, B. A. King, G. U. Bublitz and S. G. Boxer, *Proc. Natl. Acad. Sci. U. S. A.*, 1996, **93**, 8362–8367.

24 A. L. Sobolewski and W. Domcke, *Phys. Chem. Chem. Phys.*, 2004, **6**, 2763–2771.

25 L. M. Tolbert and K. M. Solntsev, *Acc. Chem. Res.*, 2002, **35**, 19–27.

26 J. E. Kwon and S. Y. Park, *Adv. Mater.*, 2011, **23**, 3615–3642.

27 J. Zhao, S. Ji, Y. Chen, H. Guo and P. Yang, *Phys. Chem. Chem. Phys.*, 2012, **14**, 8803–8817.

28 N. Nishina, T. Mutai and J. Aihara, *J. Phys. Chem. A*, 2017, **121**, 151–161.

29 C.-H. Wu, L. J. Karas, H. Ottosson and J. I. Wu, *Proc. Natl. Acad. Sci. U. S. A.*, 2019, **116**, 20303–20308.

30 B. J. Lampkin, Y. H. Nguyen, P. B. Karadakov and B. VanVeller, *Phys. Chem. Chem. Phys.*, 2019, **21**, 11608–11614.

31 L. D. Mena, D. M. A. Vera and M. T. Baumgartner, *RSC Adv.*, 2020, **10**, 39049–39059.

32 L. Gutiérrez-Arzaluz, F. Cortés-Guzmán, T. Rocha-Rinza and J. Peón, *Phys. Chem. Chem. Phys.*, 2015, **17**, 31608–31612.

33 L. J. Karas, C.-H. Wu, H. Ottosson and J. I. Wu, *Chem. Sci.*, 2020, **11**, 10071–10077.

34 Y. Zhao and D. G. Truhlar, *Theor. Chem. Acc.*, 2008, **120**, 215–241.

35 B. O. Roos, P. R. Taylor and P. E.-M. Siegbahn, *Chem. Phys.*, 1980, **48**, 157–173.

36 T. Shiozaki, W. Györffy, P. Celani and H.-J. Werner, *J. Chem. Phys.*, 2011, **135**, 081106.

37 A. Stanger, *J. Org. Chem.*, 2006, **71**, 883–893.

This journal is © the Owner Societies 2022

Phys. Chem. Chem. Phys., 2022, **24**, 11496–11500 | **11499**

38 E. Matito, J. Poater, M. Duran and M. Solà, *J. Mol. Struct.*, 2005, **727**, 165–171.

39 I. Casademont-Reig, E. Ramos-Cordoba, M. Torrent-Sucarrat and E. Matito, in *Aromaticity: Modern Computational Methods and Applications*, ed. I. Fernández, Elsevier, 2021, pp. 235–258.

40 P. Bultinck, M. Rafat, R. Ponec, B. Van Gheluwe, R. Carbó-Dorca and P. Popelier, *J. Phys. Chem. A*, 2006, **110**, 7642–7648.

41 F. Feixas, E. Matito, J. Poater and M. Solà, *J. Comput. Chem.*, 2008, **29**, 1543–1554.

42 M. Solà, F. Feixas, J. O. C. Jiménez-Halla, E. Matito and J. Poater, *Symmetry*, 2010, **2**, 1156–1179.